Draft version January 25, 2024
Typeset using LaTeX **twocolumn** style in AASTeX631

Semblance study of force-field and convection-diffusion solutions with observations of solar magnetic phenomena

M. Enríquez-Vargas[1] and Jorge U. Pérez Romero[2]

[1] *Instituto de Ciencias Físicas, Universidad Nacional Autónoma de México, 62210, Cuernavaca, Morelos, México*
[2] *Facultad de Ingeniería, Universidad Nacional Autónoma de México, 04510, Ciudad de México, México*

ABSTRACT

A quantitative analytical model based on the semblance method between the modulation factor with solar phenomena is proposed. Different Local Interstellar Spectra (LIS) have been computed to introduce into a transport equation solution which in turn have been introduced into the atmospheric yield function (Caballero-Lopez & Moraal 2012), that allows to compute a Cosmic Rays (CR) Modulation Factor. The results were as expected; there are correlation between modulation factor and sunspots, and anticorrelation between modulation factor and mean magnetic field.

A transport equation's solution is necessary to compute atmospheric yield function, in this case the used transport equation's solutions were convection-diffusion and force field. Both solutions offer similar models, yet the force field solution shows a higher correlation value in the semblance than the convection-diffusion solution.

Several LIS were also computed because they are introduced into the transport equation solutions. The used LIS were Lagner, Potgieter and Webber LIS in 2003, Burguer and Potgieter LIS in 2000, Garcia-Munoz, Mason and Simpson LIS in 1975 and Ghelfi, Barao, Derome and Maurin LIS in 2017. Those LIS were used because they have a model for different nuclear composition: Helium and Hydrogen. The LIS with more changes when is introduced into the semblance is Garcia-Munoz, Mason and Simpson in 1975.

The atmospheric yield function also need data from some neutron detectors that have changes according their cut-off rigidity value, hence two analyses were made. In the first analysis were selected three stations from different locations: close from the Arctic Circle as OULU station, in the Antarctic as SNAE and close of the equator as AATB station. In the second analysis, five different stations were averaged by arithmetic mean to observe and analyze what is the general behaviour of arrival cosmic rays on the Earth. The computed semblance models are very similar with significant differences that are shown in an analysis of zeros.

Many images were produced when the analyses were computed, then the main images, that are used as examples, are shown along the paper, while the rest can be found in the appendix.

Keywords: Cosmic Rays — Convetion-Diffusion solution — Force field solution — Semblance — Geophysics — Local interstellar spectal — Atmospheric yiel funtion

1. INTRODUCTION

To generate the proposed model, data from neutron monitors were utilized and diverse local interstellar spectra were computed. These spectra were introduced into the atmospheric yield function to determine the cosmic ray modulation factor.

Cosmic rays are electrically charged particles capable of reaching velocities as high as the speed of light, in other words, they are atoms, that lack electrons and contain high amounts of energy. Primary cosmic radiation is composed of protons, α-particles (two protons and two neutrons), $^{-4}$He and heavy nuclei.

[1] Computational resources can be found in https://github.com/JorUrie/TRC.git

Cosmic rays enter to the Earth's magnetosphere and other layers from all directions (primary cosmic rays). The primary CRs collide with particles in the Earth's atmosphere, these violent collisions cause particles to break down into smaller particles (secondary cosmic rays). This process is repeated multiple times until the particles lose sufficient energy to become elemental particles or are unable to break down due to energy loss. This phenomenon is known as an air shower (Auger et al. 1939).

High-energy cosmic rays are produced by stochastic collisions within a magnetically turbulent plasma such as a supernova, and there are also low-energy cosmic rays from similar stars to our Sun (Sekido & Elliot 1985).

Cosmic rays originating from sources beyond our solar system are detected on Earth's surface, and their detection is affected by solar activity, which is reliant on the solar cycles. Furthermore, the Sun also generates cosmic rays within its corona.

The semblance has been used to compute the desired model. Semblance is a geophysical tool mainly used in exploration seismology and it can be defined as a correlation in Fourier terms or other transform between two traces, that is, semblance is a measure to compute the similarity between two traces.

2. TRANSPORT EQUATION

The used solutions of transport equation in this document is based in Caballero-Lopez and Moraal (Caballero-Lopez & Moraal 2004) article.

The Parker's equation is given by:

$$\frac{\partial f}{\partial t} + \frac{1}{4\pi p^2}\nabla \cdot \vec{S} + \frac{1}{p^2}\frac{\partial}{\partial p}(p^2 \dot{p}) f = Q \tag{1}$$

where S is the current differential density:

$$\vec{S} = 4\pi p^2 (C\vec{V} f - K \cdot \nabla f) \tag{2}$$

The equation 1 is in terms of the omnidirectional distribution function $f(r; P; t)$, p is the particle's moment, t is the time, r is the radial distance, Q is the source of cosmic rays and V the solar wind speed. K is the diffusion tensor, that contains a parallel component $k_{\parallel}$, perpendicular $k_{\perp}$ and transverse k_T and they describe the drifts. In the equation 2, C (from the equation 3) is known as the Compton-Getting factor (Gleeson & Axford 1968). This factor was introduced into the transport equation, because the flow, which is isotropic in the reference system at rest and is not the same in the solar wind system.

$$C = -\frac{1}{3}\frac{\partial ln f}{\partial ln p} \tag{3}$$

The adiabatic energy loss is denoted as:

$$\dot{p} = -\frac{p}{3}\nabla \cdot \vec{V} \tag{4}$$

Substituting 3 and 4 in 1 two possible solutions could be gotten:

$$\frac{\partial f}{\partial t} + \nabla \cdot (\underbrace{C\vec{V} f}_{a} \underbrace{- K \cdot \nabla f}_{b}) + \underbrace{\frac{1}{p^2}\frac{\partial}{\partial p}\left[p^2 \left(\frac{p}{3}\vec{V} \cdot \frac{\nabla f}{f}\right)\right]}_{c} f = Q \tag{5}$$

3. FORCE FIELD

In the equation 5 the term a corresponds to the convection, b to the diffusion and drifts of the cosmic rays and c are the changes of energy. To solve the previous equation, different approximations have been considered. If steady state, without sources and neglect the energy losses is assumed, from the equation 5 can be obtained:

$$CVf - K \cdot \nabla f = cte = 0 \tag{6}$$

For the equation 6 is valid, the term of adiabatic losses of the equation 7 is required to be smaller than the terms convective and diffusive:

- $Vr = k << 1$ valid for high energy cosmic rays, since k is proportional to energy.
- $(1/f)\partial f/\partial r << C/r$ valid for small r, this means, in the internal heliosphere.

Considering spherical symmetry, 8 is:

$$CVf - k\frac{\partial f}{\partial r} = 0 \tag{7}$$

The force field equation can be rewrite in terms of rigidity knowing that $P = cp/q$:

$$\frac{\partial f}{\partial r} + \frac{VP}{3k}\frac{\partial f}{\partial P} = 0 \tag{8}$$

From:

$$df(r, P) = \frac{\partial f}{\partial r}dr + \frac{\partial f}{\partial P}dP \tag{9}$$

dividing by dr:

$$\frac{df}{dr} = \frac{\partial f}{\partial r}dr + \frac{\partial f}{\partial P}\frac{dp}{dr} \tag{10}$$

Considering the equation 8:

$$df = 0 \tag{11}$$

The equation 11 implies that $f(r, p)$ is constant, equal to its value at the boundary, along an outline with characteristic equation $dP/dr = VP/3k$, in the space (r, P). In the second term of the equation 8, the quantity VP/k has units of potential per unit length, that is, field units, that is why it is called a force field solution. Considering the diffusion coefficient with the form:

$$k(r, P) = \beta k_1(r) k_2(P) \tag{12}$$

the solution of the characteristic equation remains as:

$$\int_P^{P_b(r,P)} \frac{\beta\left(P'\right) k_2\left(P'\right)}{P'} dP' = \int_r^{r_b} \frac{V\left(r'\right)}{3k_1(r')} dr' \equiv \phi(r) \tag{13}$$

where ϕ is the force field parameter. When $k2 \propto P$ and $\beta \approx 1$, the solution is reduced to the most commonly form utilized:

$$\phi = P_b - P \tag{14}$$

4. CONVECTION-DIFFUSION

From the equation 5, Q is not the adiabatic loss in a rest system:

$$Vf - k\frac{\partial f}{\partial r} = 0 \tag{15}$$

The outcome is:

$$f = f_b e^{-M} \tag{16}$$

Where $M = \int_r^{r_b} \frac{V dr}{k}$ is the modulation function, ϕ is the force field parameter. Its outcome is:

$$M = \frac{3\phi}{\beta k_2} \tag{17}$$

Where M does not have unites.

Both solutions are introduced into the atmospheric yield solution, which is necessary to compute the modulation factor. However LIS is also necessary in order to compute the atmospheric yield solution.

5. LOCAL INTERSTELLAR SPECTRAL

The Local Interstellar Spectrum is a mathematical model created from observations or simulations that describe the arriving of the Cosmic Rays at outside the Heliosphere in energy terms.

The used LIS in these analyses were Lagner, Potgieter & Webber LIS in 2003, Burguer & Potgieter LIS in 2000, Garcia-Munoz, Mason & Simpson LIS in 1975 and Ghelfi, Barao, Derome & Maurin LIS in 2017.

5.1. *Lagner, Potgieter & Webber LIS in 2003*

This LIS is based on analytic solution of the Parker equation (Parker 1965), in Voyager 1, Voyager 2 and Pioneer data at 70 Astronomical Units (AU) close to the Terminal Shock (TS) during minimum solar between 1987 and 1997.

The modulation developed by Parker included drift effects, that are related to the polarity of solar magnetic field:

$$\begin{aligned}\frac{\partial f}{\partial t} =& -(V + \langle v_D \rangle) \cdot \nabla f + \nabla \cdot (K_S \cdot \nabla f) \\ &+ \frac{1}{3}(\nabla \cdot V)\frac{\partial f}{\partial InP} + j_{source}\end{aligned} \tag{18}$$

Where j_{source} is the local source. Into the equation was introduced parallel, perpendicular, and asymmetric drift coefficients to describe the gradient and derivates of curvature in large-scale Heliosphere Magnetic Field (HMF).

The local sources are not considered and dependent time into spherical coordinates system like a combination model of diffusive shock acceleration and drift modulation in two spatial dimensions, neglecting any azimuthal dependence and contemplating that is symmetric around the equatorial field (Langner et al. 2003). The model offers several CR intensities that are interpreted as particles made of different composition. When the modulation is close or outside from TS is computed in rigidity terms. The protons model is the following:

$$J_H = \frac{2.1E_{\frac{k}{n}}^{-2.8}}{1 + 5.85E_{\frac{k}{n}}^{-1.2} + 1.18E_{\frac{k}{n}}^{-2.54}} \tag{19}$$

And the Helium model is:

$$J_H = \frac{1.075E_{\frac{k}{n}}^{-2.8}}{1 + 3.9E_{\frac{k}{n}}^{-1.09} + 0.90E_{\frac{k}{n}}^{-2.54}} \tag{20}$$

5.2. *Burguer & Potgieter LIS in 2000*

The LIS was compared to ULYSSES data from September 1994 to July 1995 with a Fast Scanning of Latitude (FSL). The Parker equation was analytically solved considering an omnidirectional distribution (two dimensions), the source is located 100 UA, the Solar Wind's (SW) velocity is 400 $\frac{km}{s}$ in equatorial plane and is increasing to $800\frac{km}{s}$ in polar zones. The HMF angle sheet is 15°, which is a good value to fit for solar modulation. The model was computed by Bibber (Bieber 1999):

$$f_{IS}(R) = \left\{ \begin{array}{cc} 1.9 \times 10^4 R^{-2.78} & If\ R \geq 7GV \\ \exp(9.472 - 1.999R - 0.6938R^2 + 0.2988R^3 - (& \\ 0.04714R^4) & If\ R < 7\ GV \end{array} \right) \tag{21}$$

The model can also be expressed in terms of proton composition:

$$J_H = \frac{1.9 \times 10^4 P^{-2.78}}{1 + 0.4866P^{-2.51}} \tag{22}$$

$$J_{He} = \frac{\left(3.8 \times 10^4 P^{-2.78}\right)}{(1 + 0.9732P^{-2.51})} \tag{23}$$

5.3. *Garcia-Munoz, Mason and Simpson LIS in 1975*

To compute this LIS was consulted IMP-5, IMP-7, and IMP-8 data, because the satellites can capture several particles and their energy rage is wider, then the select data were electron $> 100MeV$ with quiet-time measurements.

The Parker's equation was analytically solved considering symmetric spherical coordinates system in stationary state and drawing on Fisk method (Fisk et al. 1974). The LIS is the following:

$$j = A(T + Bexp(-CT))^{\gamma} \tag{24}$$

Where j is particle flux, T is kinetic energy and parameters are showing in the table 1:

Species	A	B	C	γ
H	9.9×10^8	780	2.5×10^-4	2.65
^4He	1.4×10^8	660	1.4×10^-4	2.77
C	1.8×10^6	620	5.2×10^-4	2.68

Table 1: Equation 7 parameters Garcia-Munoz et al. (1975)

5.4. *Ghelfi, Barao, Derome and Maurin LIS in 2017*

Used data were AMS-01 and AMS-02, BESS-Polar and PAMELA, because they were recent (in that epoch), but Voyager 1 data was also considered.

First, the author purposes the simplest modulation model to link unmodulated (IS) to modulated (TOA) qualities, that is a force field approximation Ghelfi et al. (2017):

$$\frac{E^{TOA}}{A} = \frac{E^{IS}}{A} - \frac{|Z|}{A}\phi \tag{25}$$

$$J^{TOA}\left(E^{TOA}\right) = \left(\frac{p^{TOA}}{p^{IS}}\right)^2 \times J^{IS}\left(E^{IS}\right) \tag{26}$$

Where E is total energy, p is the momentum, and $J \equiv \frac{dJ}{dE_{\frac{k}{n}}}$ is the differential flux per kinetic energy per nucleon $E_{\frac{k}{n}}$.

An analysis χ^2 was necessary to fix the TOA flux with all the species $N_j(i)$ in this t_j, over all possible energy $E_k(i,\ j)$ and is giving by:

$$\chi^2 = \sum_{t_i}\sum_{N_{j(i)}}\sum_{E_{k(i,j)}} \frac{\left(J^{TOA}\left(J_j^{IS},\ \phi_j, E_k\right) - data_{ijk}\right)^2}{\sigma_{ijk}} \tag{27}$$

Where IS parameters are free. For the previous mentioned was used power laws in total energy (O'Neill 2006) or rigidity (Shikaze et al. 2007). TOA data for H and He are old and have more inconsistencies than new data, thus has applied a χ^2 analysis to minimize errors, therefore was used package MINUIT minimisation package (James 1998) from Root CERN libraries Sartini et al. (2010). Markov Chain Monte Carlo analysis (MCMC) was implemented from the GreAT package (Putze & Derome 2014) to determine the correlation between credible intervals for ϕ and IS flux. MCMC analysis is based on Bayes theorem. Finally, all the obtained data is represented as an interpolated logarithmic-polynomial function, which is shown in the equation 28.

$$\log_{10}\left(J_{IS}\right) = \begin{cases} \sum_{i=0}^{12} c_i \left(\frac{\log_{10}\left(E_{\frac{k}{n}}\right)}{\log_{10}\left(800\,\frac{GeV}{n}\right)}\right)^i & \text{if } E_{\frac{k}{n}} < 800\frac{GeV}{n} \\ C_0 - C_1\left(\frac{\log_{10}\left(E_{\frac{k}{n}}\right)}{\log_{10}\left(800\,\frac{GeV}{n}\right)}\right) & \text{if } E_{\frac{k}{n}} \geq 800\frac{GeV}{n} \end{cases} \tag{28}$$

In this paper were just applied four LIS, however more models were also considered, and it is worthwhile to mention them.

5.5. *Boschini, Della Torre, Gervasi and more LIS in 2018*

For the calculation of this LIS was used GALPROP and HeldMod to simulate CR data, but real data was required, so Voyager 1, BESS, PAMELA, AMS-01 and AMS-02 data were consulted.

GALPROP code use astronomical, particle physics and nuclear information to predict CR flux, X-ray, synchrotron emissions and their polarisation (Strong et al. 2007). Heliosphere propagation was computed by GALPROP and thanks to MCMC analysis, data was more realistic, after the information was introduced in HelMod program to obtain modulated data.

Previous data was compared with real information from the satellites with different energy content. The used information was a combination of Voyager 1, AMS-02, CREAM-I and ATIC-02, but CREAM-I and AMS-02 had better adjust because they offer minimal error. To compute the analytical LIS was used MCMC analysis from Eureqa[1] and the analytical model take the next form:

$$F(R)\times R^{2.7} = \begin{cases} \sum_{i=0}^{5} a_i R^i & R \leq 1GV \\ b + \frac{c}{R} + \frac{(d_1)}{d_2+R} + \frac{(e_1)}{e_2+R} + \frac{(f_1)}{f_2+R} + & \\ gR & R \geq 1GV \end{cases} \tag{29}$$

Where the parameters are showing in the table 2.

	a_0	a_1	a_2	a_3	a_4	a_5	b	c	d_1	d_2	e_1	e_2	f_1	f_2	g
p	94.1	-831	0	16700	-10200	0	10800	8590	-4230000	3190	274000	17.4	-39400	0.464	0
H	1.14	0	-118	578	0	-87	3120	-5530	3370	1.29	134000	88.5	-1170000	861	0.03

Table 2. Equation 12 parameters (Boschini et al. 2017)

5.6. *Vos & Potgieter LIS in 2015*

The LIS was computed using observations from several PAMELA data during a solar minimum of 2006 to 2009. This LIS was computed from the Parker equation (Parker 1965), which was solved as a ray distribution function in rigidity terms, time, position in 3D, in a heliocentric spherical coordinates where polar angles is equal to 90°. All short-term modulation effects are neglected (solar minimum conditions), average particle drift velocity is caused by gradients and curvature in Heliospheric Magnetic Field (HMF), there is a symmetric diffusion tensor and adiabatic energy changes except in heliosheath (Potgieter et al. 2012).

The LIS is the following (Vos & Potgieter 2015):

$$j_{LIS} = 2.70\left(\frac{E^{1.12}}{\beta^2}\right)\left(\frac{E+0.67}{1.67}\right)^{-3.93} \tag{30}$$

Where E is kinetic energy, $\beta = \frac{v}{c}$ particle velocity (like light velocity), $j_{LIS} = P^2 f$.

5.7. *Moskalenko, Strong, Ormes and Potgieter LIS in 2002*

Cosmic Ray data was simulated by DTUNUC Monte Carlo code (Ferrari et al. 1996) and data was recollected from two previous works (Tan & Ng 1983) and (Tan & Ng 1983). The Parker equation (Parker 1965) was solved through Crank-Nicholson numerical solution (Crank & Nicolson 1947) and accorded with the author a model more realistic was sought, then leaky box code was applied (weighted-slab). GALPROP was also used to compute 3D cosmic rays.

[1] http://www.nutonian.com/products/eureqa/

The Helium LIS was approximated to a Force Field, because of low energy approximation of the ϕ potential modulation has been selected using the CLIMAX neutron monitor.

To ensure that the spectrum is similar to the simulated values, a power law dependent on kinetic energy based on the convection-diffusion solution has been approximated, which cannot only be described by a single function.

Finally, the LIS was subjected to a χ_n^2 function to observe the quality of the adjusted data for each individual measurement (Moskalenko et al. 2002) is just shown in the equation 31:

$$J_H = \begin{cases} \exp\left(4.64 - 0.08\left(\log\left(E_{\frac{k}{n}}\right)\right)^2 - 2.91\sqrt{E_{\frac{k}{n}}}\right), \\ E_{\frac{k}{n}} \leq 1GeV \\ \exp\left(3.22 - 2.86\log\left(E_{\frac{k}{n}}\right) - \frac{1.5}{E_{\frac{k}{n}}}\right), \\ E_{\frac{k}{n}} > 1GeV \end{cases} \tag{31}$$

The LIS previously mentioned are shown in the figure 2 into the rigidity purpose parameters by each author:

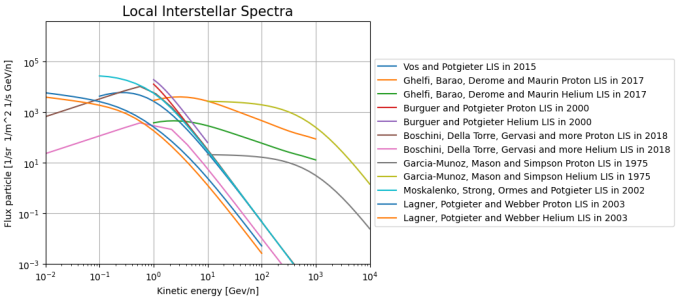

Figure 2: Local Interstellar Spectral purpose by different authors.

6. SEMBLANCE

The semblance is the cross-relation between two traces, the computed value is interpreted as the similarity of two points contained in the signals that lie in the Fourier domain, however in this analysis was used Continuous Wavelet Transform (CWT) that represents a wave in two dimensions and measure the similarity between two signals.

CWT is given:

$$CWT(u,s) = \int_{-\infty}^{\infty} h(t)\frac{1}{|s|^{0.5}}\Psi^*\left(\frac{t-u}{s}\right)dt \tag{32}$$

Where s is scale, u is displacement, Ψ is the mother wavelet , and * means complex conjugate and t is the coordinate in time (Cooper & Cowan 2008) the equation 32 can also be expressed in spatial terms (Teolis 2017):

$$\Psi(x) = \frac{1}{\pi f_b}e^{2\pi i f_c x}e^{-\frac{x^2}{f_b}} \tag{33}$$

The conventional semblance is a normalized coherence measure, first computed in 1969 (Taner & Koehler 1969) A time later, Neidell and Taner (Neidell & Taner 1971) found, that the coherence and semblance were two different operators, so semblance was expressed as shown in the equation 34:

$$S_{NT}\ [i] = \frac{\sum_{j=i-M}^{i+M}\left(\sum_{k=0}^{N-1} q[j,k]\right)^2}{N\sum_{j=i-M}^{i+M}\sum_{k=0}^{N-1} q[j.k]^2} \tag{34}$$

where $i,\ j$ are time sample indices, k is a trace number, $q[j,\ k]$ is the trace amplitude at time index j a trace number k of the NMO-corrected gather.

To reduce and make more smoothly the decays often is applied a boxcar filter, that can be rewritten as (Luo et al. 2015):

$$S_C\ [i] = \frac{\sum_j h[i-j]\left(\sum_k q[j,k]\right)^2}{N\sum_j h[i-j]\sum_k q[j.k]^2} \tag{35}$$

There is an alternative expression for the conventional semblance, that can be expressed as a normalized correlation coefficient, but first a trace $r[j]$ should be defined as a summation over trace number:

$$r[j] \equiv \sum_k q[j,k] \tag{36}$$

Therefore:

$$C_{rq}[i] \equiv \sum_j h[i-j]\sum_k r[j]q[j,k] \tag{37}$$

$$C_{rr}[i] \equiv \sum_j h[i-j]\sum_k r[j]^2 \tag{38}$$

$$C_{qq}[i] \equiv \sum_j h[i-j]\sum_k q[j,k]^2 \tag{39}$$

Now, the three equations 37, 38 and 39 can be rewritten as a conventional semblance (Luo et al. 2015):

$$S_C[i] = \frac{C_{rq}[i]^2}{C_{rr}[i]C_{qq}[i]} \tag{40}$$

7. COUNT RATES FROM GROUND-BASED DETECTORS

The neutrons detected at ground level are the product of atmospheric showers caused by the collision of a primary particle, that collides with a molecule in the atmosphere. The neutron count is given by the following equation:

$$N\left(P_c,\ \ x,\ \ t\right) = \int_{P_c}^{\infty}\left(\frac{-dN}{dP}\right)dP = \sum_i\int_{P_c}^{\infty} S_i(P,\ x)j_i(P,t)dP \tag{41}$$

Where $j_i(P,t)$ is the spectrum of the primary species above the atmosphere, and $S_i(P,x)$ is the atmospheric yield function due to this species. P_c is the cut-off rigidity, which is the necessary minimum energy for a particle to enter the Earth's magnetosphere. The quantity $dN = dP$ is the differential counting rate of the instrument inside the atmosphere. The

yield function, that was used in this analysis is the following (Caballero-Lopez & Moraal 2012):

$$S_H = \frac{-(dN/dP)}{J_H(P) + 1.584F(P)j_{He}} \tag{42}$$

where $F(P)$ is the ratio between the yield functions of He and H reported by (Clem & Dorman 2000):

$$F(P) = F_0(P_0^a + P^a)^{(\gamma_1 - \gamma_2/a)} P\gamma^2 \tag{43}$$

the values in the equation are: $F_0 = 2.0$, $\gamma_1 = 0$, $\gamma_2 = 10$, $a = 1.4$ and $P_0 = 0.45$.

The equation 42 allows to compute a modulation factor and will be used to obtain the semblance. The J_H and J_{He} terms in the equation 42 are the transport equation solution (convection-diffusion or force field) that are in terms of a LIS previously mentioned. A code on Python has been programmed and can be found here: https://github.com/JorUrie/TRC.git

8. FIRST ANALYSIS

The first analysis consists in three stations located in different latitudes (Table **??**) and compute their modulation factor, then semblance between modulation factor with sunspots or mean solar magnetic field will be computed. Data were downloaded from the Neutron Monitor DataBase (NMDB)[2], sunspots data from Sunspot Number[3] (Figure 3) and mean solar magnetic field from The Wilcox Solar Observatory[4] (Figure 4).

Neutron Monitor	Cut-off Rigidity [Counts/seg]
SNAE	0.73
OULU	0.81
AATB	5.90

Table 2: Cut-off Rigidity from the stations used in the first analysis

[2] NMDB
[3] Sunspot Number | SILSO (sidc.be)
[4] WSO - The Wilcox Solar Observatory (stanford.edu)

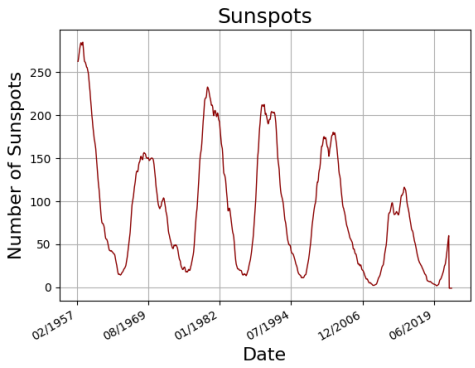

Figure 3: Sunspots data obtained from Sunspot index and Long-term Solar Observations.

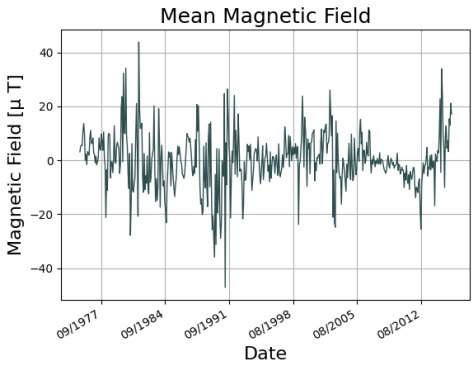

Figure 4: Solar Magnetic Field date obtained from The Wilcox Solar Observatory

The Figure 3 is about the number of sunspots recorded, that are related to solar maximum and minimum. Data is from May, 1957 to July, 2022. In the same figure, solar cycles can be observed, in other words, solar maximums belong to the years 1958, 1970, 1980, 1990, 2014 and the next solar maximum could be in 2024. Solar minimum belongs to the years 1965, 1976, 1986, 1997 and 2010. With the previous information, 11-year cycle can be perceived. In 1958 was the larggest recorded maximum, while the smallest maximum was in 1970, as soon as minimums have similar values and there are not much differences.

Mean magnetic field information belongs to the dates from May 1975 to December 2015. The information has cusps and looks to not have changes, but in September 1981 was the biggest registered maximum, while in March 1991 was the smaller registered value. If a line is traced along the graphic following a "regression", maximums and minimums could be seen, they would be mostly inversely proportionate to sunspots.

The selected stations were SNAE (south), OULU (north) and AATB (equator). They were deemed appropriate based on their respective latitudes in Earth (Figure 24). SNAE, OULU and AATB data are showed in the figures 5, 6 and 7. Data were downloaded and normalized by contained higher value.

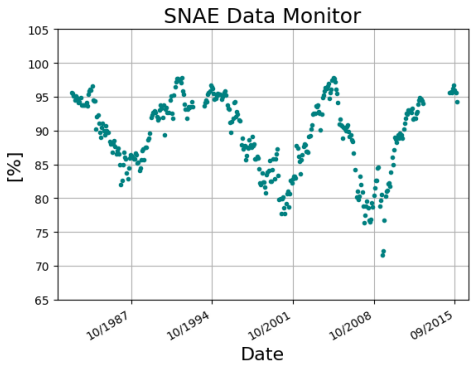

Figure 5: SNAE data obtained from NMDB.

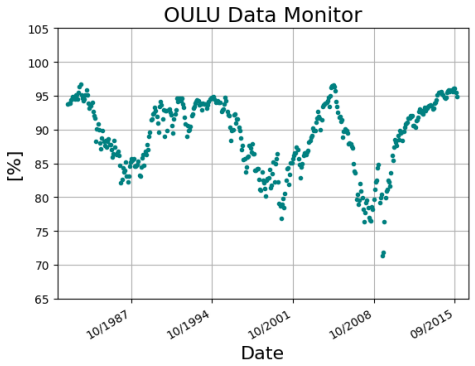

Figure 6: OULU data obtained from NMDB.

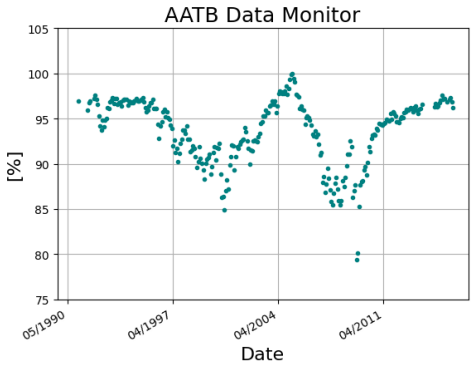

Figure 7: AATB data obtained from NMDB.

The previous mentioned figures 5, 6 and 7 are normalized data, because the data is obtained from the neutral monitors on the Earth, however the particles have already modified by modulation phenomena and they have also lost energy (secondary cosmic rays), for that reason a modulation factor is necessary to compute.

Non-normalised data have been introduced into the atmospheric yield function, which requires a LIS and a transport equation solution (convection-diffusion or force field) to compute the modulation factor.

The figures from 8 to 15 are the modulation factors for the same station with every previously mentioned LIS and a transport equation solution. Their unities are $Counts/s$ and $Date$, because the modulation factor is the amount of particles before to enter the atmosphere and be influenced by particles or the magnetosphere of the Earth (primary species) in a given date. Modulation factor would not be necessary if the satellites would take desired measurements, but the technology and the conditions do not allow it.

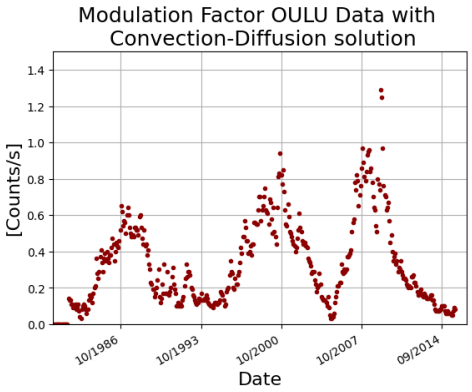

Figure 8: OULU station. Modulation factor with Convection-Diffusion solution using Lagner, Potgieter and Webber LIS in 2003.

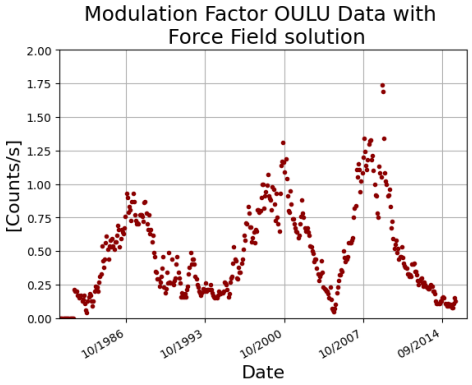

Figure 9: OULU station. Modulation factor with Force Field solution using Lagner, Potgieter and Webber LIS in 2003.

The previous compute was applied to all selected stations. The spectral modulation factors have a similar pattern for each LIS and are also similar to the downloaded data, for example, the figure 6 and figure 8, can be observed the high values in 1987, near to 2004 and 2011, those occurred for the figures 8 to 15, in fact for the figures 8, 10, 12 and 14 between values 1.2 and 1.4 $Counts/s$, two points are always present and are also the highest values. For the figures 9, 11, 13 and 15, they have the same pattern and the two highest points are also present, but between 1.5 and 1.75 $Counts/s$, so the difference of the spectral modulation factors using convection-diffusion solution and force field solution is the amplitude.

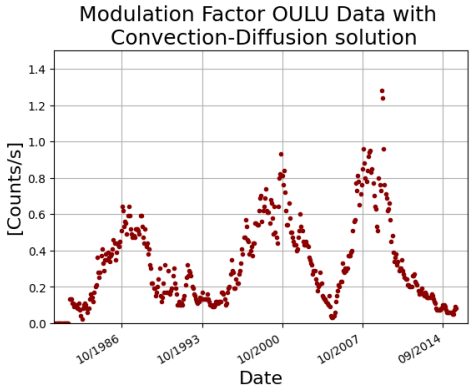

Figure 10: OULU station. Modulation factor with Convection-Diffusion solution using Burguer and Potgieter LIS in 2000.

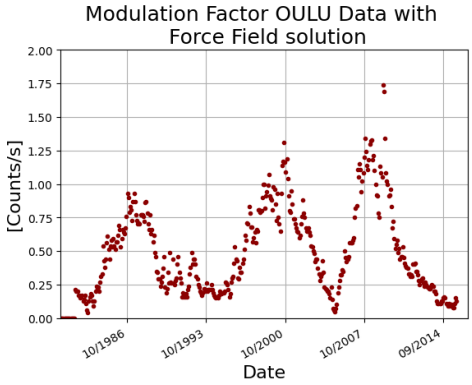

Figure 11: OULU station. Modulation factor with Force Field solution using Burguer and Potgieter LIS in 2000.

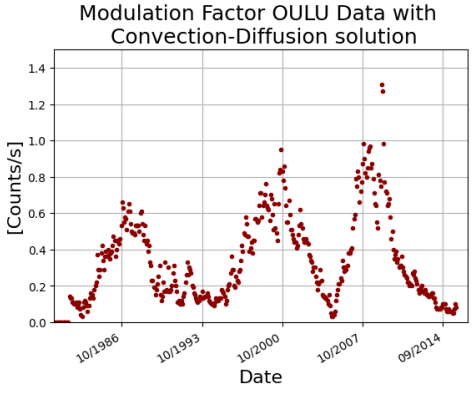

Figure 12: OULU station. Modulation factor with Convection-Diffusion solution using Garcia-Munoz, Mason and Simpson LIS in 1975.

From the figures 8 to 15 also looks like to the figure 3, because there are more extragalatic cosmic rays introduced into the Earth as a result of the low solar modulation.

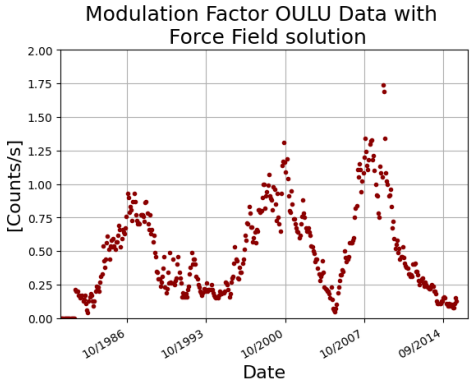

Figure 13: OULU station. Modulation factor with Force Field solution using Garcia-Munoz, Mason and Simpson LIS in 1975.

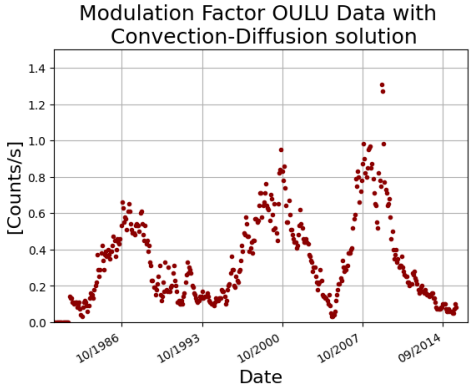

Figure 14: OULU station. Modulation factor with Convection-Diffusion solution using Ghelfi, Barao, Derome and Maurin LIS in 2017.

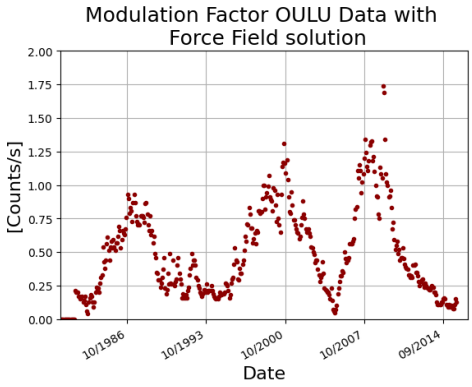

Figure 15: OULU station. Modulation factor with Force Field solution using Ghelfi, Barao, Derome and Maurin LIS in 2017.

For the three stations, that have been selected according to their latitude, the semblance between modulation factor

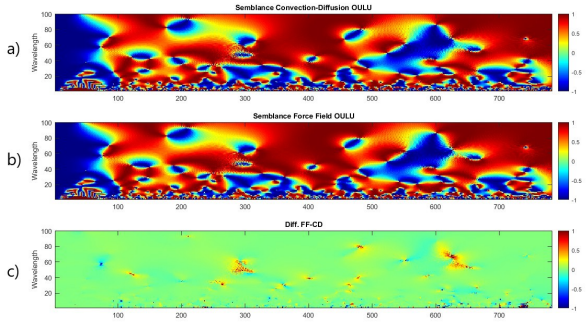

Figure 16: OULU Station a) Semblance between Modulation Factor using Convection-Diffusion with Lagner, Potgieter and Webber LIS in 2003 vs Sunspot data. b) Semblance between Modulation Factor using Force Field with Lagner, Potgieter and Webber LIS in 2003 vs Sunspot data. c) Difference between the two previous semblances.

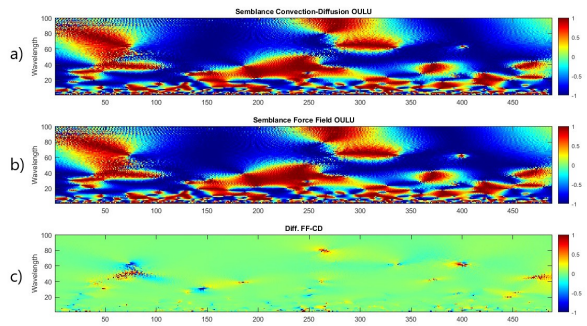

Figure 17: OULU Station a) Semblance between Modulation Factor using Convection-Diffusion with Lagner, Potgieter and Webber LIS in 2003 vs Mean Magnetic Field data. b) Semblance between Modulation Factor using Mean Magnetic Field with Lagner, Potgieter and Webber LIS in 2003 vs Sunspot data. c) Difference between the two previous semblances.

and sunspots using several LIS are showed, however only for OULU station, the rest models can be found in the appendix.

The computed models offer similar results among them (figures *a*) and *b*) for each semblance figure), they even look like if they were the same model, but thanks to the difference between semblances (figures *c*)) is possible to observe, that there are little differences mainly in the figures 21 and 20. If both figures previously mentioned are comparative with the rest of respective semblances in this section, the main difference is in the interval 50 to 100 in horizontal axis and 40 to 80 in the wavelength, where blue spot change his size and form.

There is correlation between sunspots and modulation phenomena, which can be observed in the figures 16, 18, 20 and 22 highlighted in red. There is anti-correlation between

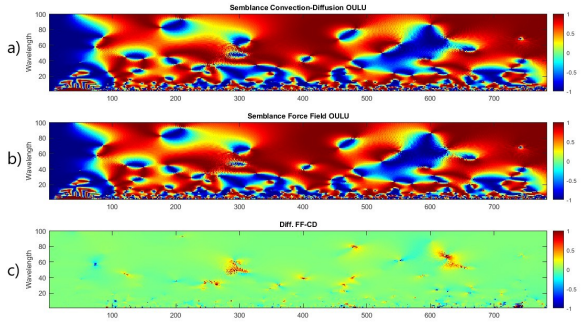

Figure 18: OULU Station a) Semblance between Modulation Factor using Convection-Diffusion with Burguer and Potgieter LIS in 2000 vs Sunspot data. b) Semblance between Modulation Factor using Force Field with Burguer and Potgieter LIS in 2000 vs Sunspot data. c) Difference between the two previous semblances.

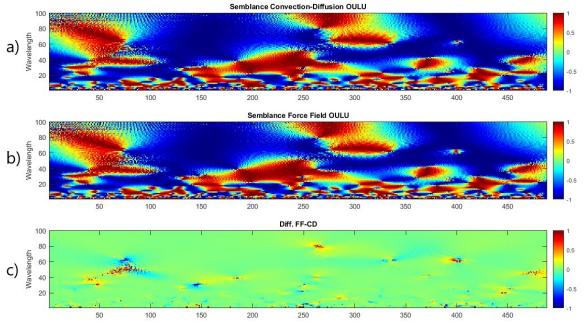

Figure 19: OULU Station a) Semblance between Modulation Factor using Convection-Diffusion with Burguer and Potgieter LIS in 2000 vs Mean Magnetic Field data. b) Semblance between Modulation Factor using Force Field with Burguer and Potgieter LIS in 2000 vs Mean Magnetic Field data. c) Difference between the two previous semblances.

the mean solar magnetic field and the modulation phenomena observed in blue colour. Both behaviours are maintained independently of the Earth's latitude.

9. SECOND ANALYSIS

The same calculus was performed, but the spectral factor modulations were average while taking into account the LIS. The data from the following stations were used: KERG, MOSC, OULU, THUL, and HRMS (Table ??).

The Figure 24 are the position of the used stations in both analyses.

The Figures 25 to 32 are the spectral averaged using convection-diffusion and force field solutions with Lagner, Potgieter & Webber LIS in 2003, Burguer & Potgieter LIS in 2000, Garcia-Munoz, Mason & Simpson LIS in 1975 and Ghelfi, Barao, Derome & Maurin LIS in 2017.

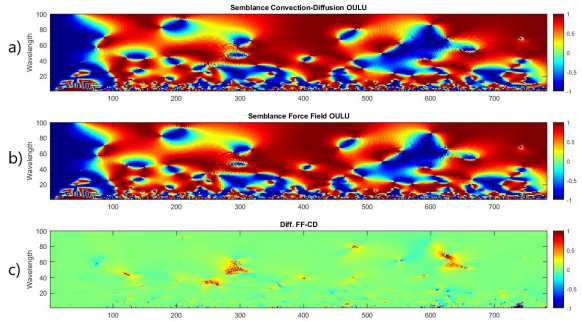

Figure 20: OULU Station a) Semblance between Modulation Factor using Convection-Diffusion with Garcia-Munoz, Mason and Simpson LIS in 1975 vs Sunspot data. b) Semblance between Modulation Factor using Force Field with Garcia-Munoz, Mason and Simpson LIS in 1975 vs Sunspot data. c) Difference between the two previous semblances.

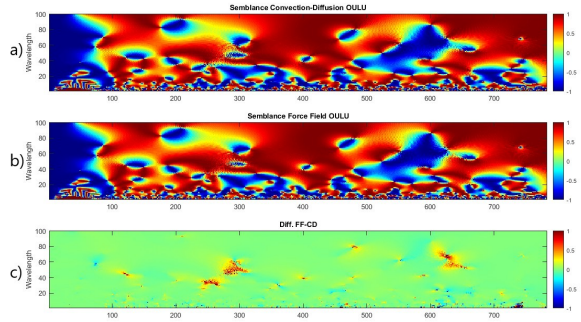

Figure 22: OULU Station a) Semblance between Modulation Factor using Convection-Diffusion with Ghelfi, Barao, Derome and Maurin LIS in 2017 vs Sunspots data. b) Semblance between Modulation Factor using Force Field with Ghelfi, Barao, Derome and Maurin LIS in 2017 vs Sunspots data. c) Difference between the two previous semblances.

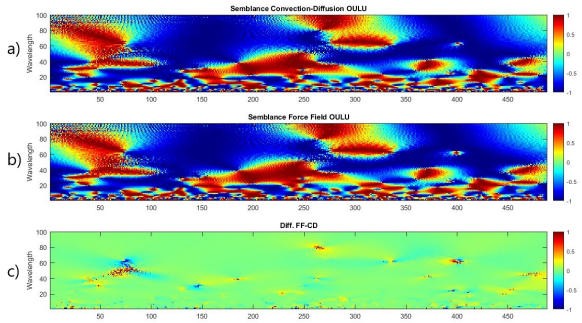

Figure 21: OULU Station a) Semblance between Modulation Factor using Convection-Diffusion with Garcia-Munoz, Mason and Simpson LIS in 1975 vs Mean Magnetic Field data. b) Semblance between Modulation Factor using Force Field with Garcia-Munoz, Mason and Simpson LIS in 1975 vs Mean Magnetic Field data. c) Difference between the two previous semblances.

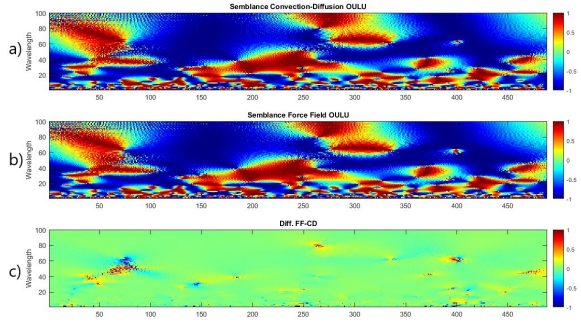

Figure 23: OULU Station a) Semblance between Modulation Factor using Convection-Diffusion with Ghelfi, Barao, Derome and Maurin LIS in 2017 vs Mean Magnetic Field data. b) Semblance between Modulation Factor using Force Field with Ghelfi, Barao, Derome and Maurin LIS in 2017 vs Mean Magnetic Field data. c) Difference between the two previous semblances.

Neutron Monitor	Cut-off Rigidity [Counts/seg]
THUL	**0.3**
OULU	**0.81**
KERG	**1.14**
MOSC	**2.43**
HRMS	**4.58**

Table 3: Cut-off Rigidity from the used stations in the second analysis

The Figures 33 to 48 are the semblance between the aforementioned modulation factors with sunspots and mean magnetic field data. The figures 34, 36, 38, 40 and 42 are the percentage of contained zeros into the difference between semblance (Figures *c*)), that were calculated to observed with more detail which LIS has the best adjusted in order to find the most reliable model.

In this case, an average modulation factor of several neutron detectors around the word was computed to analyse the general behaviour between sunspots and mean solar magnetic field with modulation phenomena. The results were utterly similar to the first analysis, in fact the analysis of the contained zeros confirms the hypothesis, that there is correlation between sunspots and modulation phenomena and anti-correlation between the mean magnetic field and modulation phenomena. The analysis of the zeros can be summarised in the Table **??**.

Analysis of contained zeros	Sunspots		Mean Magnetic Field	
	<0	>0	<0	> 0
Webber & Lockwood	47	53	46	54
Burguer	47	53	46	54
Garcia-Munoz	49	51	47	53
Maurin	49	51	46	54

Table 4: Analysis of contained zeros from difference between semblance using transport equation solution convection-diffusion and force field and different LIS

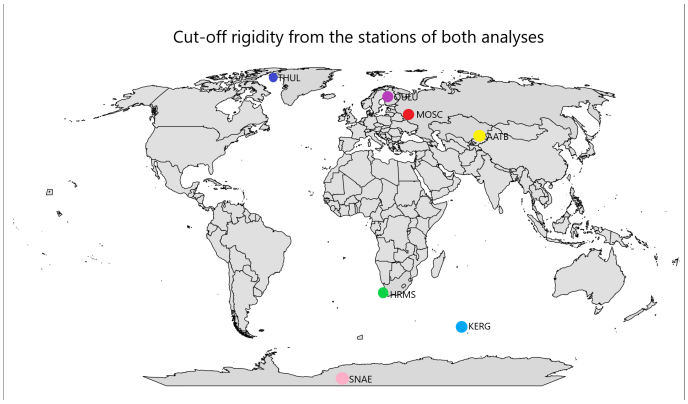

Figure 24: Position of the neutron monitors around the world used in both analyses

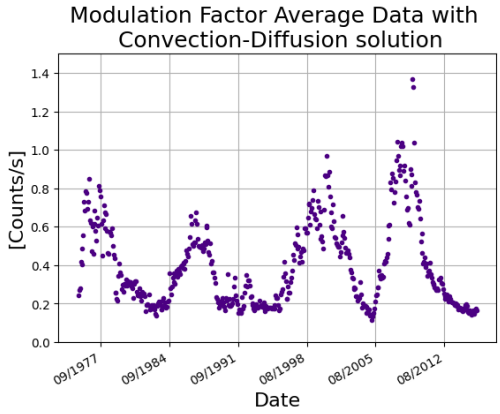

Figure 25: Averaged Modulation Factor among KERG, HRMS, MOSC, OULU and THUL stations. Modulation factor with Convection-Diffusion solution using Lagner, Potgieter & Webber LIS in 2003.

10. CONCLUSIONS

Both analyses allow quantifying the correlation between modulation factor with sunspots and anti-correlation between modulation factor with mean magnetic field. The models are mostly similar with both transport equation solutions and the local interstellar spectrum, because just shown light changes.

For the first analysis, the modulation factors yield similar outcomes and are solely dependent on the rigidity factor. The correlation between sunspots and modulation factor is more pronounced for stations closer to the poles, such as OULU and SNAE, than the equatorial AATB station. However, this pattern is not replicated for the semblance between the modulation factor and the mean magnetic field. The station near the equator shown more anti-correlation than near the poles. The pattern is similar for every semblances, which were used different LIS and transport equation solution.

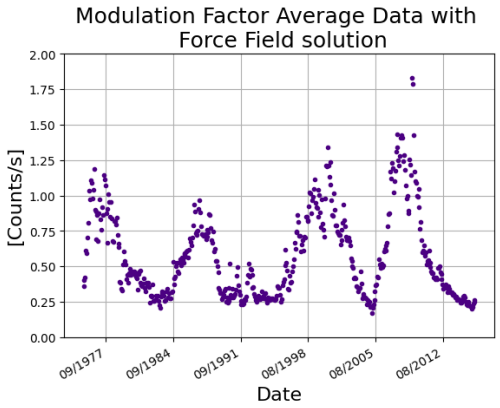

Figure 26: Averaged Modulation Factor among KERG, HRMS, MOSC, OULU and THUL stations. Modulation factor with Force Field solution using Lagner, Potgieter & Webber LIS in 2003..

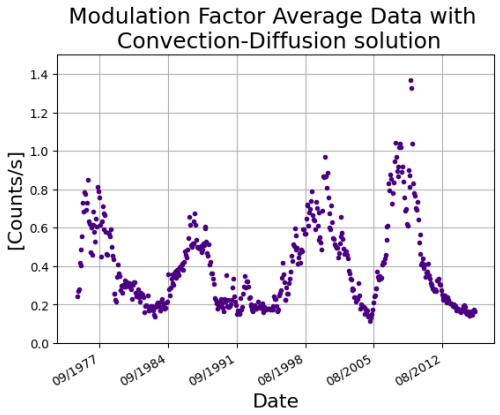

Figure 27: Averaged Modulation Factor among KERG, HRMS, MOSC, OULU and THUL stations. Modulation factor with Convection-Diffusion solution using Burguer and Potgieter LIS in 2000.

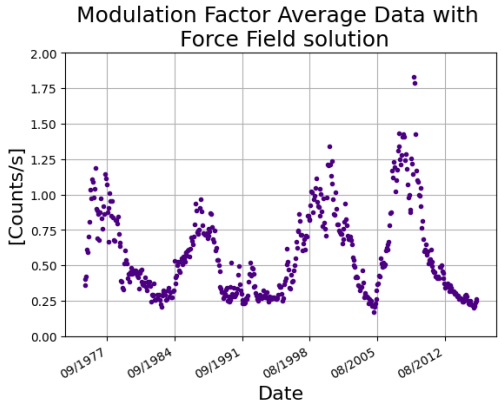

Figure 28: Averaged Modulation Factor among KERG, HRMS, MOSC, OULU and THUL stations. Modulation factor with Force Field solution using Burguer and Potgieter LIS in 2000.

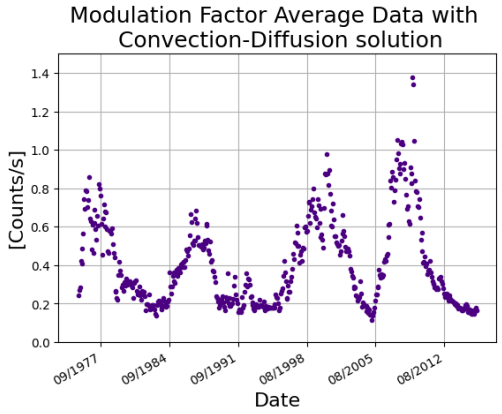

Figure 29: Averaged Modulation Factor among KERG, HRMS, MOSC, OULU and THUL stations. Modulation factor with Convection-Diffusion solution using Garcia-Munoz, Mason and Simpson LIS in 1975.

Thanks to the second analysis, the first analysis could be affirmed and generalized, the force field solution is also more compatible with neutron detectors data, Additionally any modulation factor solution will be similar to the Neutron detector data and just will have minimal amplitude variations.

In the second analysis, it is possible to observe similarity among the graphs of contained zeros into the difference of semblances, particularly when the modulation factors have been computed by different LIS. However if semblance is computed using the Garcia-Munoz, Mason and Simpson LIS in 1975 shown more differences, that is visible in the analysis of contained zeros for semblance between averaged modulation factor and mean magnetic field.

According to the table ?? semblance between sunspots and averaged modulation factors are really similar and the percentage of contained zeros are akin if Webber & Lockwood and Burguer and Potgieter LIS in 2000 are used, same

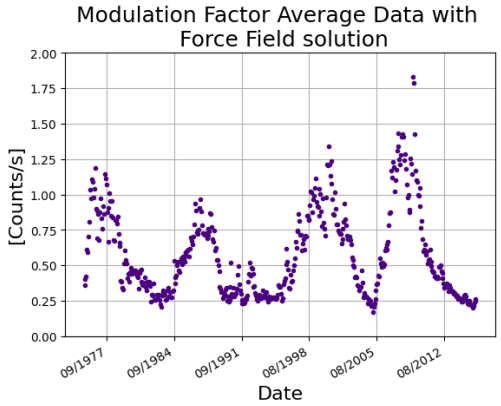

Figure 30: Averaged Modulation Factor among KERG, HRMS, MOSC, OULU and THUL stations. Modulation factor with Force Field solution using Garcia-Munoz, Mason and Simpson LIS in 1975.

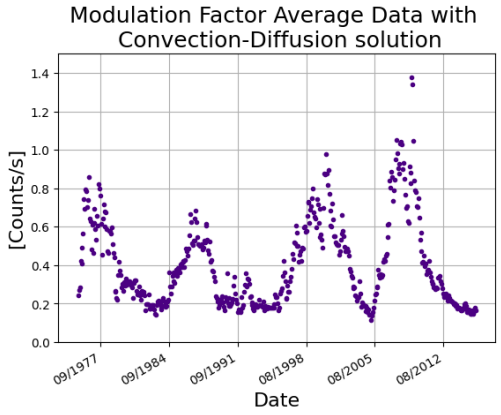

Figure 31: Averaged Modulation Factor among KERG, HRMS, MOSC, OULU and THUL stations. Modulation factor with Convection-Diffusion solution using Ghelfi, Barao, Derome and Maurin LIS in 2017.

happened for Garcia-Munoz and Ghelfi, Barao, Derome and Maurin LIS in 2017.

Therefore, the LIS that have the best adjust to the semblance model are Lagner, Potgieter and Webber LIS in 2003, Burguer and Ghelfi, Barao, Derome and Maurin LIS in 2017 using force field solution because they offer more consistent values as shown in the table ??.

With both proposed models can be asserted with greater certainty that exist a correlation between modulation phenomena and sunspots, because the solar activity is less allowed to detect more rays from the Sun. The anti-correlation between modulation phenomena and mean magnetic field is due to the high solar activity, therefore there are less solar rays that affect the arisen of cosmic rays from others source.

Thanks to this proposed quantitative model, a more precise predictive model of cosmic rays with solar activity can be compute.

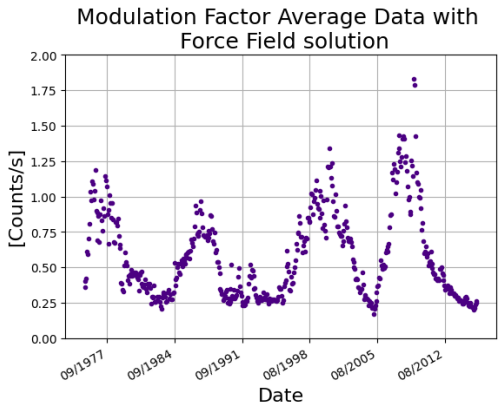

Figure 32: Averaged Modulation Factor among KERG, HRMS, MOSC, OULU and THUL stations. Modulation factor with Force Field solution using Ghelfi, Barao, Derome and Maurin LIS in 2017.

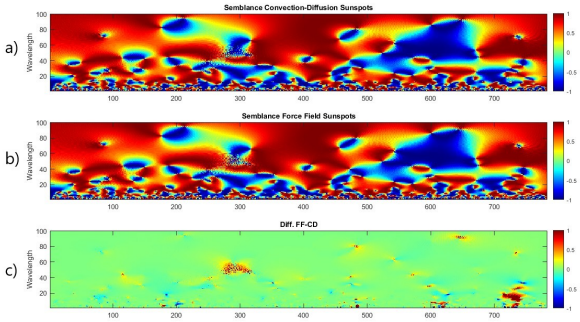

Figure 33: Average among HRMS, KERG, MOSC, OULU and THUL a) Semblance between Average Modulation Factor using Convection-Diffusion with Lagner, Potgieter and Webber LIS in 2003 vs Sunspots data. b) Semblance between Average Modulation Factor using Force Field with Lagner, Potgieter and Webber LIS in 2003 vs Sunstpots data. c) Difference between the two previous semblances.

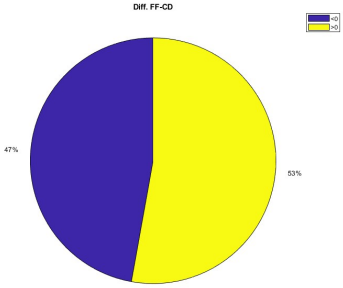

Figure 34: Contained zeros into Figure 33 c).

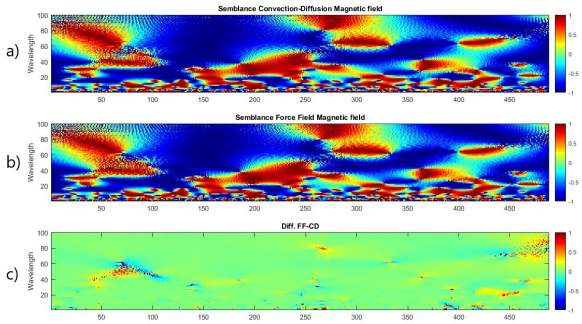

Figure 35: Average among HRMS, KERG, MOSC, OULU and THUL a) Semblance between Average Modulation Factor using Convection-Diffusion with Lagner, Potgieter and Webber LIS in 2003 vs Solar Magnetic Field data. b) Semblance between Average Modulation Factor using Force Field with Lagner, Potgieter and Webber LIS in 2003 vs Solar Magnetic Field data. c) Difference between the two previous semblances.

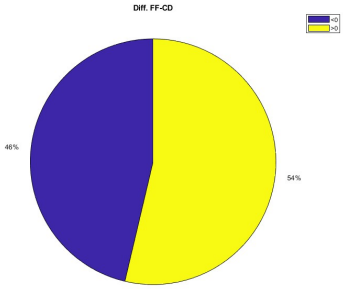

Figure 36: Contained zeros into Figure 35 c).

REFERENCES

Auger, P., Ehrenfest, P., Maze, R., Daudin, J., & Fréon, R. A. 1939, Reviews of Modern Physics, 11, 288, doi: 10.1103/RevModPhys.11.288

Bieber, J. 1999, in International Cosmic Ray Conference, Vol. 7, 26th International Cosmic Ray Conference (ICRC26), Volume 7, 61

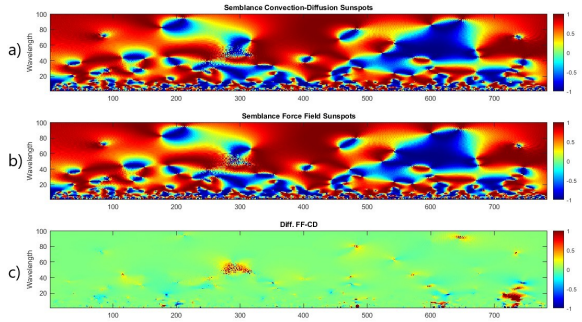

Figure 37: Average among HRMS, KERG, MOSC, OULU and THUL a) Semblance between Average Modulation Factor using Convection-Diffusion with Burguer and Potgieter LIS in 2000 vs Sunspots data. b) Semblance between Average Modulation Factor using Force Field with Burguer and Potgieter LIS in 2000 vs Sunstpots data. c) Difference between the two previous semblances.

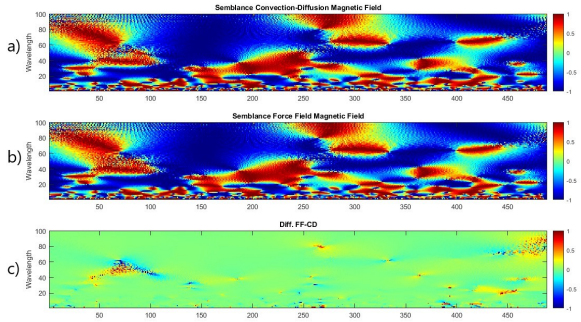

Figure 39: Average among HRMS, KERG, MOSC, OULU and THUL a) Semblance between Average Modulation Factor using Convection-Diffusion with Burguer and Potgieter LIS in 2000 vs Solar Magnetic Field data. b) Semblance between Average Modulation Factor using Force Field with Burguer and Potgieter LIS in 2000 vs Solar Magnetic Field data. c) Difference between the two previous semblances.

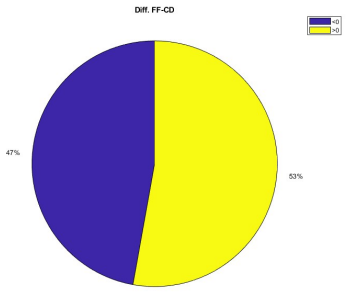

Figure 38: Contained zeros into Figure 37 c).

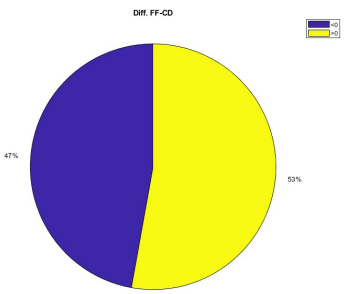

Figure 40: Contained zeros into Figure 39 c).

Boschini, M. J., Della Torre, S., Gervasi, M., et al. 2017, ApJ, 840, 115, doi: 10.3847/1538-4357/aa6e4f

Caballero-Lopez, R. A., & Moraal, H. 2004, Journal of Geophysical Research: Space Physics, 109, doi: https://doi.org/10.1029/2003JA010098

—. 2012, Journal of Geophysical Research: Space Physics, 117, doi: https://doi.org/10.1029/2012JA017794

Clem, J., & Dorman, L. 2000, Space Science Reviews, 93, doi: 10.1023/A:1026508915269

Cooper, G. R. J., & Cowan, D. R. 2008, Computers and Geosciences, 34, 95, doi: 10.1016/j.cageo.2007.03.009

Crank, J., & Nicolson, P. 1947, Mathematical Proceedings of the Cambridge Philosophical Society, 43, 50–67, doi: 10.1017/S0305004100023197

Ferrari, A., Ranft, J., Roesler, S., & Sala, P. R. 1996, Zeitschrift für Physik C: Particles and Fields, 71, 75, doi: 10.1007/s002880050149

Fisk, L. A., Goldstein, M. L., Klimas, A. J., & Sandri, G. 1974, ApJ, 190, 417, doi: 10.1086/152893

Garcia-Munoz, M., Mason, G. M., & Simpson, J. A. 1975, ApJ, 202, 265, doi: 10.1086/153973

Ghelfi, A., Barao, F., Derome, L., & Maurin, D. 2017, Astronomy & Astrophysics, 605, C2, doi: 10.1051/0004-6361/201527852e

Gleeson, L. J., & Axford, W. I. 1968, Canadian Journal of Physics Supplement, 46, 937, doi: 10.1139/p68-388

James, F. a. 1998. https://cds.cern.ch/record/2296388

Langner, U. W., Potgieter, M. S., & Webber, W. R. 2003, Journal of Geophysical Research: Space Physics, 108, doi: https://doi.org/10.1029/2003JA009934

Luo, X., Zhang, M., Potgieter, M., Feng, X., & Pogorelov, N. V. 2015, ApJ, 808, 82, doi: 10.1088/0004-637X/808/1/82

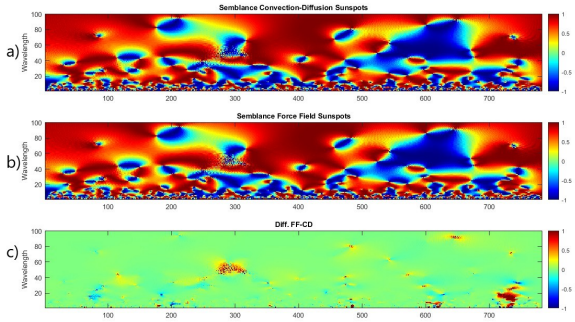

Figure 41: Average among HRMS, KERG, MOSC, OULU and THUL a) Semblance between Average Modulation Factor using Convection-Diffusion with Garcia-Munoz, Mason and Simpson LIS in 1975 vs Sunspots data. b) Semblance between Average Modulation Factor using Force Field with Garcia-Munoz, Mason and Simpson LIS in 1975 vs Sunstpots data. c) Difference between the two previous semblances.

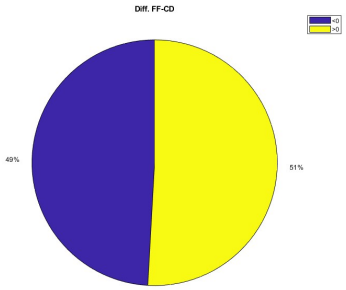

Figure 42: Contained zeros into Figure 41 c).

Moskalenko, I. V., Strong, A. W., Ormes, J. F., & Potgieter, M. S. 2002, The Astrophysical Journal, 565, 280, doi: 10.1086/324402

Neidell, N. S., & Taner, M. T. 1971, GEOPHYSICS, 36, 482, doi: 10.1190/1.1440186

O'Neill, P. M. 2006, Advances in Space Research, 37, 1727, doi: 10.1016/j.asr.2005.02.001

Parker, E. N. 1965, Planet. Space Sci., 13, 9, doi: 10.1016/0032-0633(65)90131-5

Potgieter, M., De Simone, N., Vos, E., Boezio, M., & Di Felice, V. 2012, in 39th COSPAR Scientific Assembly, Vol. 39, 1526

Putze, A., & Derome, L. 2014, Physics of the Dark Universe, 5, 29, doi: 10.1016/j.dark.2014.07.002

Sartini, L., Simeone, F., Pani, P., et al. 2010, Nuclear Instruments and Methods in Physics Research A

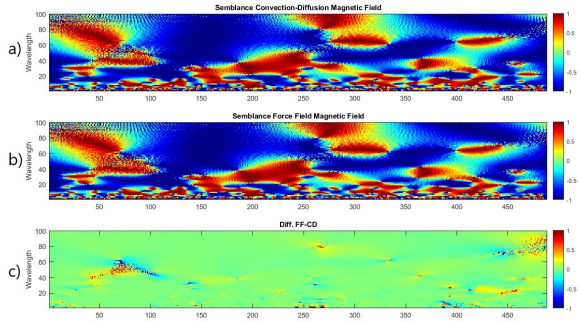

Figure 43: Average among HRMS, KERG, MOSC, OULU and THUL a) Semblance between Average Modulation Factor using Convection-Diffusion with Garcia-Munoz, Mason and Simpson LIS in 1975 vs Solar Magnetic Field data. b) Semblance between Average Modulation Factor using Force Field with Garcia-Munoz, Mason and Simpson LIS in 1975 vs Solar Magnetic Field data. c) Difference between the two previous semblances.

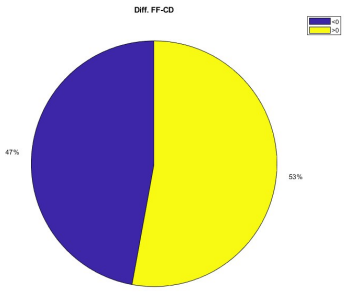

Figure 44: Contained zeros into Figure 43 c).

Sekido, Y., & Elliot, H. 1985, Early history of cosmic ray studies: Personal reminiscences with old photographs. https://www.osti.gov/biblio/7169147

Shikaze, Y., Haino, S., Abe, K., et al. 2007, Astroparticle Physics, 28, 154, doi: 10.1016/j.astropartphys.2007.05.001

Strong, A. W., Moskalenko, I. V., & Ptuskin, V. S. 2007, Annual Review of Nuclear and Particle Science, 57, 285, doi: 10.1146/annurev.nucl.57.090506.123011

Tan, L. C., & Ng, L. K. 1983, ApJ, 269, 751, doi: 10.1086/161084

Tan, L. C., & Ng, L. K. 1983, Journal of Physics G: Nuclear Physics, 9, 227, doi: 10.1088/0305-4616/9/2/015

Taner, M. T., & Koehler, F. 1969, GEOPHYSICS, 34, 859, doi: 10.1190/1.1440058

Teolis, A. 2017, Computational Signal Processing with Wavelets, doi: 10.1007/978-3-319-65747-9

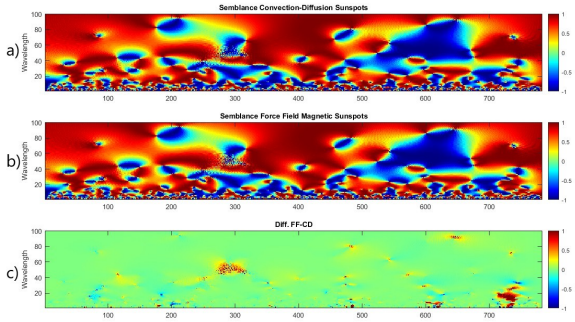

Figure 45: Average among HRMS, KERG, MOSC, OULU and THUL a) Semblance between Average Modulation Factor using Convection-Diffusion with Ghelfi, Barao, Derome and Maurin LIS in 2017 vs Sunspots data. b) Semblance between Average Modulation Factor using Force Field with Ghelfi, Barao, Derome and Maurin LIS in 2017 vs Sunstpots data. c) Difference between the two previous semblances.

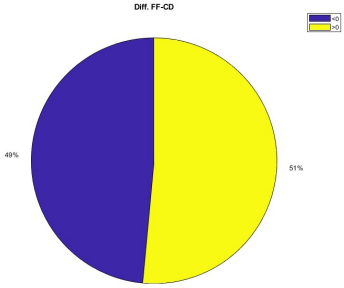

Figure 46: Contained zeros into Figure 45 c).

Vos, E. E., & Potgieter, M. S. 2015, ApJ, 815, 119,

doi: 10.1088/0004-637X/815/2/119

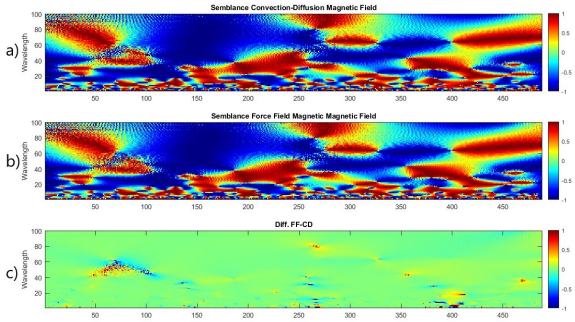

Figure 47: Average among HRMS, KERG, MOSC, OULU and THUL a) Semblance between Average Modulation Factor using Convection-Diffusion with Ghelfi, Barao, Derome and Maurin LIS in 2017 vs Solar Magnetic Field data. b) Semblance between Average Modulation Factor using Force Field with Ghelfi, Barao, Derome and Maurin LIS in 2017 vs Solar Magnetic Field data. c) Difference between the two previous semblances.

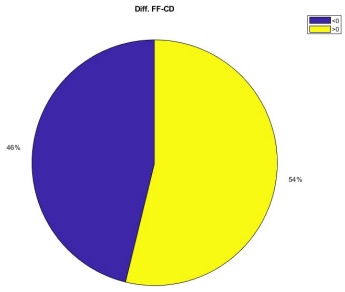

Figure 48: Contained zeros into Figure 47 c).

11. APPENDIX

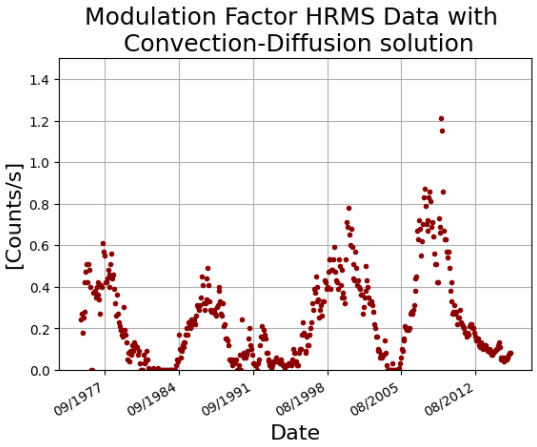

Figure 49: HRMS station. Modulation factor with Convection-Diffusion using Lagner, Potgieter & Webber LIS in 2003

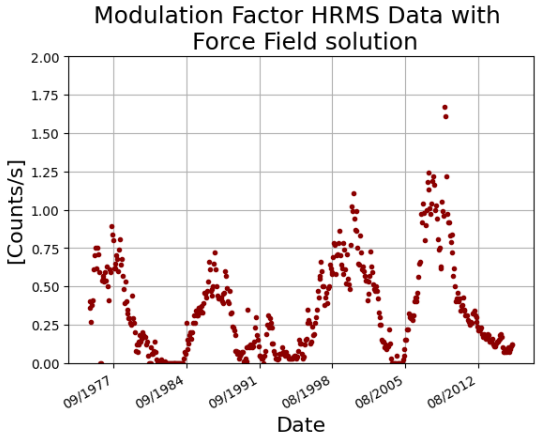

Figure 50: HRMS station. Modulation factor with Force Field using Lagner, Potgieter & Webber LIS in 2003

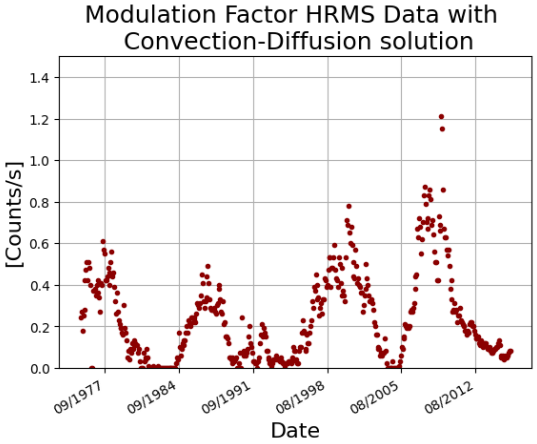

Figure 51: HRMS station. Modulation factor with Convection-Diffusion using Burguer and Potgieter LIS in 2000

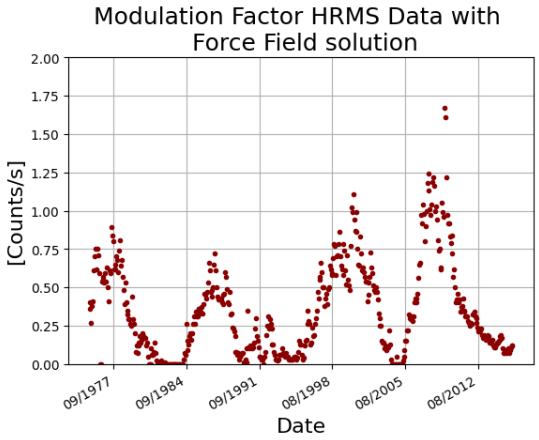

Figure 52: HRMS station. Modulation factor with Force Field using Burguer and Potgieter LIS in 2000

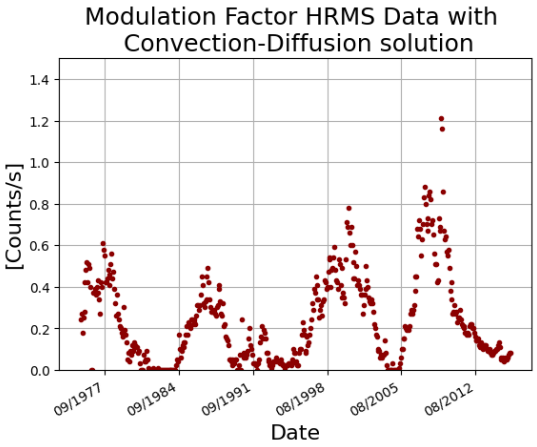

Figure 53: HRMS station. Modulation factor with Convection-Diffusion using Garcia-Munoz, Mason and Simpson LIS in 1975

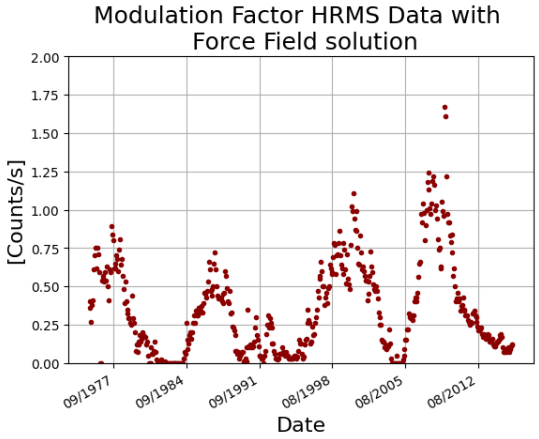

Figure 54: HRMS station. Modulation factor with Force Field using Garcia-Munoz, Mason and Simpson LIS in 1975

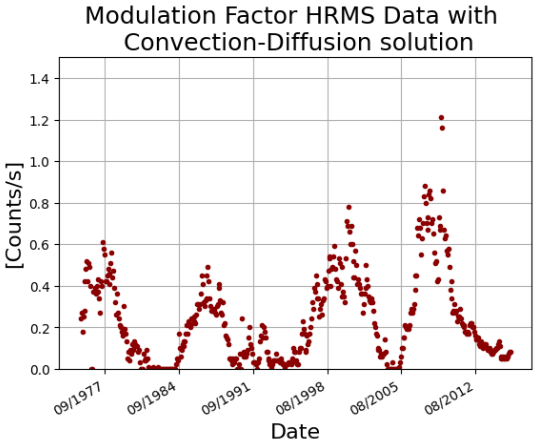

Figure 55: HRMS station. Modulation factor with Convection-Difussion using Ghelfi, Barao, Derome and Maurin LIS in 2017 in 2017

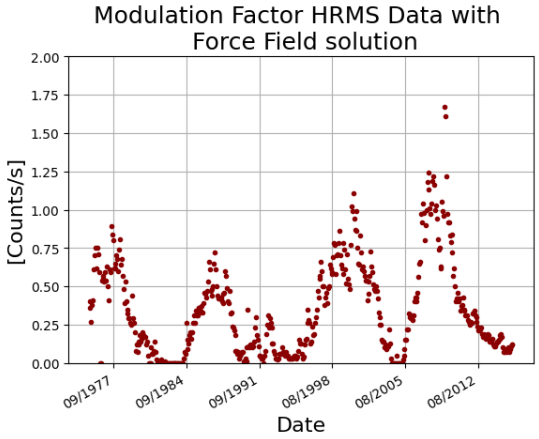

Figure 56: HRMS station. Modulation factor with Force Field using Ghelfi, Barao, Derome and Maurin LIS in 2017 in 2017

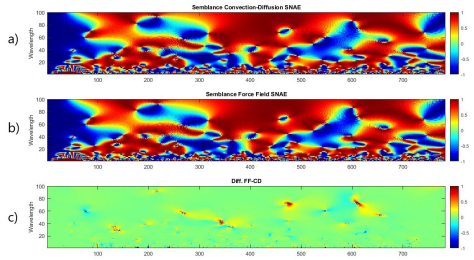

Figure 57: SNAE Station a) Semblance between Modulation Factor using Convection-Diffusion with Lagner, Potgieter and Webber LIS in 2003 vs Sunspot data. b) Semblance between Modulation Factor using Force Field with Lagner, Potgieter and Webber LIS in 2003 vs Sunspot data. c) Difference between the two previous semblances.

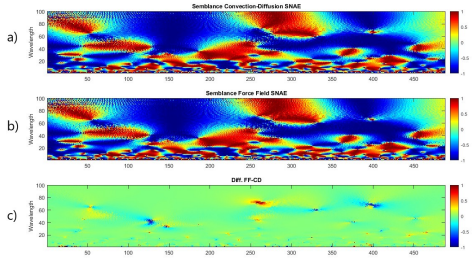

Figure 58: SNAE Station a) Semblance between Modulation Factor using Convection-Diffusion with Lagner, Potgieter and Webber LIS in 2003 vs Mean Magnetic Field data. b) Semblance between Modulation Factor using Force Field with Lagner, Potgieter and Webber LIS in 2003 vs Mean Magnetic Field data. c) Difference between the two previous semblances.

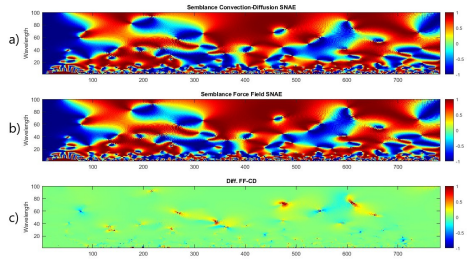

Figure 59: SNAE Station a) Semblance between Modulation Factor using Convection-Diffusion with Burguer and Potgieter LIS in 2000 vs Sunspot data. b) Semblance between Modulation Factor using Force Field with Burguer and Potgieter LIS in 2000 vs Sunspot data. c) Difference between the two previous semblances.

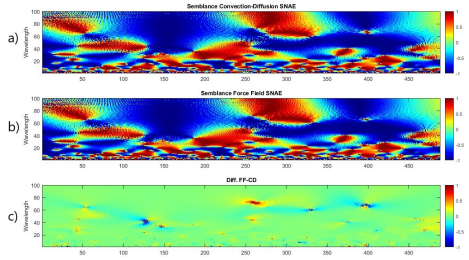

Figure 60: SNAE Station a) Semblance between Modulation Factor using Convection-Diffusion with Burguer and Potgieter LIS in 2000 vs Mean Magnetic Field data. b) Semblance between Modulation Factor using Force Field with Burguer and Potgieter LIS in 2000 vs Mean Magnetic Field data. c) Difference between the two previous semblances.

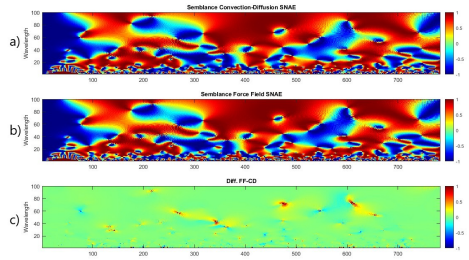

Figure 61: SNAE Station a) Semblance between Modulation Factor using Convection-Diffusion with Garcia-Munoz, Mason and Simpson LIS in 1975 vs Sunspot data. b) Semblance between Modulation Factor using Force Field with Garcia-Munoz, Mason and Simpson LIS in 1975 vs Sunspot data. c) Difference between the two previous semblances.

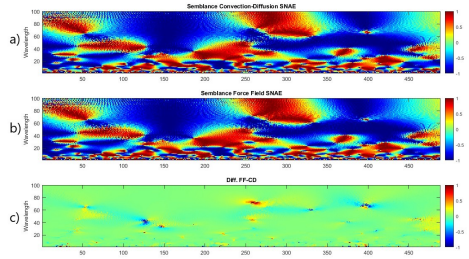

Figure 62: SNAE Station a) Semblance between Modulation Factor using Convection-Diffusion with Garcia-Munoz, Mason and Simpson LIS in 1975 vs Mean Magnetic Field data. b) Semblance between Modulation Factor using Force Field with Garcia-Munoz, Mason and Simpson LIS in 1975 vs Mean Magnetic Field data. c) Difference between the two previous semblances.

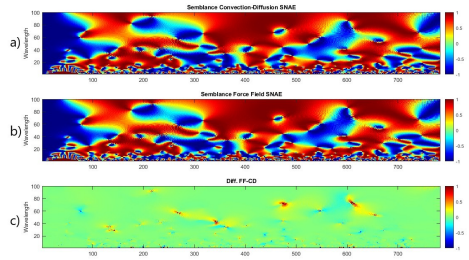

Figure 63: SNAE Station a) Semblance between Modulation Factor using Convection-Diffusion with Ghelfi, Barao, Derome and Maurin LIS in 2017 in 2017 vs Sunspots data. b) Semblance between Modulation Factor using Force Field with Ghelfi, Barao, Derome and Maurin LIS in 2017 in 2017 vs Sunspots data. c) Difference between the two previous semblances.

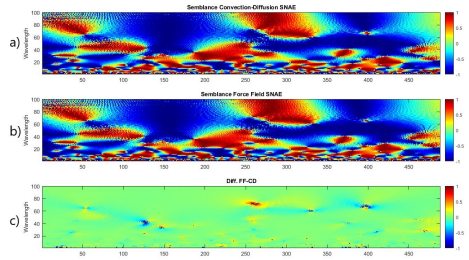

Figure 64: SNAE Station a) Semblance between Modulation Factor using Convection-Diffusion with Ghelfi, Barao, Derome and Maurin LIS in 2017 in 2017 vs Mean Magnetic Field data. b) Semblance between Modulation Factor using Force Field with Ghelfi, Barao, Derome and Maurin LIS in 2017 vs Mean Magnetic Field data. c) Difference between the two previous semblances.